

Research Article

Tribological Characteristics of Carbon Nanotubes-Reinforced Plasma-Sprayed Al_2O_3 - TiO_2 Ceramic Coatings

Chaitanya Kalangi,¹ Venkateshwarlu Bolleddu,¹ and Haiter Lenin Allasi^{1,2} 

¹Department of Manufacturing, School of Mechanical Engineering, Vellore Institute of Technology, Vellore 632014, India

²Department of Mechanical Engineering, Wollo University, Kombolcha Institute of Technology, Post Box No. 208, Kombolcha, Ethiopia

Correspondence should be addressed to Haiter Lenin Allasi; drahlenin@kiot.edu.et

Received 10 July 2021; Revised 6 August 2021; Accepted 11 August 2021; Published 7 September 2021

Academic Editor: Adam Khan M

Copyright © 2021 Chaitanya Kalangi et al. This is an open access article distributed under the Creative Commons Attribution License, which permits unrestricted use, distribution, and reproduction in any medium, provided the original work is properly cited.

Thermal-sprayed coatings are widely used in various oil and gas industries for wear and corrosion applications. However, increasing performance and requirements make conventional coatings inadequate for future needs. Furthermore, the heat conductivity of bulk materials cannot be minimized easily. Therefore, the use of low porous coating with nanocomposite doping is an effective way to produce coatings with reduced thermal conductivity. Plasma-sprayed Al_2O_3 - TiO_2 coatings are found in a wide range of applications recently in many industries because of their exceptional properties including low expenses and ease of availability. In this work, the wear-resistant and low porous coatings of $\text{Al}_2\text{O}_3 + 3 \text{ wt}\% \text{TiO}_2$ and respective carbon nanotube (CNT) doped coatings are prepared and characterized. The coatings are deposited on the AISI 1020 steel substrate using air plasma spraying. The impact of CNTs reinforcement on the percentage of pores and wear performance of coatings is investigated. Also, wear tracks morphology is investigated to determine the wear mechanism that is responsible for the wear of coatings. From the analysis, it is observed that the formation of cracks as well as micropores is decreased by the addition of carbon nanotubes. Moreover, uniform CNT distribution and good adhesion of coatings with the substrate are the major factors that improve the wear performance of the coated surface.

1. Introduction

Surface engineering plays a vital role in the reduction of wear as well as corrosion-induced damages in hi-tech industries [1, 2]. Material degradation in the service span of thermal engineering is not only disruptive but also inexpedient to the economy of production. To overcome these issues, researchers have developed a protective shield for covering the material of engineering components with feasible ceramic powder coatings. It will prolong the lifespan of a material when the coating is proved to be mechanical (high toughness and high hardness) and resistant to wear damages [3]. Various studies on ceramic coatings have been conducted to determine the mechanical properties as well as the wear resistance on the material surface. These investigations revealed that the wear resistance is greatly influenced by the

factors such as hardness, the grain size of powder, binder phase content, phase distribution, toughness, and the coating microstructure [4]. However, because of its excellent chemical strength, ceramic materials are also extensively used in different structural applications. The main key attribute of ceramic coatings is to provide wear resistance in order to achieve high hardness strength. As a result, ceramics have been increasingly utilized in the form of coatings on metallic surfaces to attain stable material characteristics [5–7]. Ceramic coatings are deposited on the surface of the metal substrates through deposition techniques. Of these, plasma-based thermal spraying (i.e., air plasma spraying, APS) is the most popular method adopted for coating deposition under high temperatures and harsh environments.

Thermal barrier coatings (TBCs) are significantly used nowadays to defend the hot section components of aircraft

engines from wear, erosion, pores, and other severe thermal degradations. An average temperature range of about 80°C and hot-spot temperature of 170°C have been reduced in the turbine blades with 250 μm thickness thermal-sprayed coating [8]. Plasma-sprayed TBCs are typically applied to increase the resistance of heat engines against wear and corrosion at a room/high temperature. The most frequently used plasma-sprayed feedstock powders in thermal barrier application are alumina-titania ($\text{Al}_2\text{O}_3\text{-TiO}_2$) and yttria-stabilized zirconia (YSZ). In recent decades, alumina-titania feedstock containing 3, 13, and 40 wt% compositions of titania are commonly used rather than plain alumina-titania powders. During spraying, these composites are heated up to 4,000°C and accelerated to several hundred m/s in a chemical dynamic environment of plasma-making gases and the surrounding atmosphere [9]. At this condition, the feedstock experiences a high thermal load, in addition to high mechanical load upon reaching the substrate. These extreme conditions can lead to substantial variations in the chemical and microstructural composition of coatings as compared to the feedstock powders and contribute to changes in coatings microstructure [10]. Additionally, alumina-titania coatings are popular due to their sliding wear resistance owing to their excellent mechanical properties. As wear undergoes aggressive corrosion at higher temperatures, the coating should be prepared in such a manner as to withstand wear and corrosion at the same time. On the other hand, TBC characteristics are mainly affected by the pores formed in the microstructure of coatings during spraying. Hence, several experiments are performed to identify the relationship between processing methods, porosity, and microstructure, resulting in properties including heat conductivity, thermal shock resistance, microhardness, fracture toughness, and so on [11, 12].

Porosity is identified as an important feature for corrosion and wear that influences the life span of hot compartments. The presence of pores in the coating is required not only for thermal conductivity reduction but also for the compensation of stress resulting from expansion because of temperature variations and heat effects [13, 14]. Nevertheless, in some cases, pores cause air penetration and gas combustion, which in turn create metal corrosion inside the parts of turbine engines [15]. Therefore, porous optimization on the top coat is significant to enhance the thermal properties for the entire lifetime of the product. The study in [16] indicated that the residual stress of coatings steadily upsurges from 60 MPa compressive stress to 40 MPa tensile stress along with the rise of porosity from 14% to 17%. Also, the authors of [17] investigated the impact of both thermal conductivity and porosity in coated surfaces. It is found that increasing the porosity could block the heat transfer between coating layers. However, low porosity would eliminate the resistance towards corrosion. The study in [18] pointed out that the reduction in thermal conductivity is possibly due to interlamellar pores occurring in the coated regions. Furthermore, it also occurs because of the limited characterization of porous shape and size, total porosity, and distribution of pores in thermal coatings.

The thickness of thermal-sprayed coatings normally ranges between 300 and 400 μm . Numerous studies revealed

that within a certain limit, the thick coatings maintain better wear resistance as well as porosity compared to thin coatings, which extends the product lifetime accordingly [19, 20]. However, thick coatings may create micropores, delamination, cracks, and improper mechanical bonding [21, 22]. Likewise, larger internal stress and other aspects will make the thick coating peel off from the coated surface [23]. Thus, thick coatings are usually difficult to be applied in practice. Wear-out failure is another main damage formed in the layers of the material substrate. Moreover, the microstructure characteristics and the wear resistance layer look uneven due to the granularity of ceramic powders. To overcome these drawbacks, the coating powder is mixed with reinforcement components that withstand wear and corrosion. In this research, $\text{Al}_2\text{O}_3 + 3 \text{ wt}\% \text{TiO}_2$ ceramic powder is reinforced with CNT nanocomposite for improving the overall wear resistance and reducing the porosity of coatings [24, 25]. The addition of carbon nanotubes is an effective way of improving the mechanical properties and tribological performance of ceramic coatings. Due to their excellent mechanical, electrical, and chemical properties, CNTs possess high tensile strength and stiffness [26]. So, CNTs applied as an additive to increase the performance of a ceramic coating in high-level industries.

Thermal barrier coatings are frequently used in heavy-duty, high-speed industrial applications for equipment protection. An integral part of TBC in a metallic substrate is to prevent the formation of large pores to reduce heat insulation and thermal stresses. However, accurate prediction of porosity is highly complex because of the challenging porous structure and the ultrathin thickness of the coating. In this paper, a conventional ceramic powder $\text{Al}_2\text{O}_3 + 3 \text{ wt}\% \text{TiO}_2$ along with 1%, 3%, and 5% CNT-doped combination of $\text{Al}_2\text{O}_3 + 3 \text{ wt}\% \text{TiO}_2$ ceramics was prepared and fabricated on the sample steel substrate via air plasma spraying deposition technique. The mechanical and wear characteristics of the coated substrate using these powders are studied and investigated. The main objective of this research is to analyze the wear response and porosity of coatings prepared with conventional ceramic and carbon nanotube mixed powders. Moreover, it investigates the influence of ceramic as well as CNTs reinforced ceramic coatings deposited on the substrate. The microstructure and tribological properties of thermal-sprayed coatings are also systematically analysed, and the wear mechanism has been determined.

2. Experimental Methodology

2.1. Materials. The coatings are deposited on the AISI 1020 steel substrate of dimension 65 \times 55 \times 5 mm. This is a medium-carbon steel substrate composed of 0.25–0.50% carbon, 0.60–1.65% manganese, 0.4% (maximal) phosphorous, and 0.5% (maximal) sulphur. Carbon steels are extensively used for large industrial applications. $\text{Al}_2\text{O}_3 + 3 \text{ wt}\% \text{TiO}_2$ powder with a particle size distribution of about 18–56 μm is taken for coating deposition. This feedstock powder is obtained from Metallizing Equipment Co. Pvt. Ltd, Jodhpur, India. In a typical thermal barrier coating system, two layers

are applied on the surface of the substrate, namely the bond coat and the top coat. Therefore, $\text{Al}_2\text{O}_3 + 3 \text{ wt}\% \text{TiO}_2$ ceramic powder is taken for deposition of the top coat, and Ni-5%Al or Ni-5%Cr ceramic powders are taken as bond coat material. The substrates are coated with both conventional ceramics as well as nanocomposite incorporated ceramics. For nanocomposite incorporated powder preparation, multiwalled carbon nanotubes (MWCNTs) are obtained from United Nanotech Innovations Pvt. Ltd., Bangalore, India. The physical properties of MWCNTs include $25 \mu\text{m}$ outer diameter, 10 microns length, >98% purity, $220 \text{ m}^2/\text{g}$ specific surface area, and $0.14 \text{ g}/\text{cm}^3$ bulk density. The blend of alumina-titania feedstock is subsequently mixed with 1%, 3%, and 5% MWCNTs of approximate diameter $25 \mu\text{m}$ and length 10 microns for 8 hours at 100 rpm speed to produce the reinforced ceramic composite powder. Agglomeration of powders during blending is avoided using hardened steel balls in the ball milling chamber. It has been learned that up to 5 wt% SiO_2 -MgO-coated MWCNTs were added with polymer for coating purposes [27].

2.2. Substrate Preparation. The AISI 1020 steel substrate is cut from a steel bar of width 55 mm and thickness 5 mm using a power saw. A surface grinder Alex NH 500 is used to remove the oxide from the top and bottom surfaces of the substrate and produce $0.1 \mu\text{m}$ roughness to the surfaces. The top surface of the substrate is grit blasted inside a suction-type cabinet of the grit-blasting machine with alumina grits of mesh size 24 at 100 psi air pressure, and a stand-off distance of 125 mm. This will provide a surface roughness of $5 \mu\text{m}$ thick, which is essential for achieving superior mechanical anchorage between the substrate and the bond coat. The oxide layers formed during the time gap between surface grinding and grit blasting processes are removed at the final stage of grit blasting. The grit blasted surface is then subjected to ultrasonic cleaning in the isopropanol bath for 10 minutes in order to remove the unwanted dirt particles from the surface. Before bond coat deposition, the wet substrate is then thermally preheated for 150–200°C using a plasma gun with argon/nitrogen as the plasma gas. This will remove oil, grease, water vapour, and foreign particles and present a clean and nascent substrate surface for the bond coat deposition. The temperature variations throughout preheating are monitored via a noncontact instrument called an optical pyrometer.

2.3. Plasma Spraying. The conventional ceramic powder of $\text{Al}_2\text{O}_3 + 3 \text{ wt}\% \text{TiO}_2$ and its corresponding CNT-doped mixtures are deposited as the top coat on the steel substrate using the plasma spraying technique. The schematic diagram of plasma-sprayed coating is depicted in Figure 1. Before the top coat deposition, the substrate is coated with an intermediate adhesion layer called a bond coat. Ni-5%Al or Ni-5%Cr composites are applied as the bond coat onto the substrate material. The coatings are deposited onto the substrate using a Sulzer Metco 3MB plasma gun fixed on a CNC X-Y table. The plasma gun uses argon and hydrogen as the primary and secondary gases, respectively. The process

parameters of the coating deposition influence the output voltage and arc power per unit hydrogen gas flow rate. A spray angle of 90° is maintained for coating all types of powder composition. Two auxiliary air jets are placed parallel to the plasma flame to cool the substrate during deposition and remove the weakly bonded and unmelted powder particles. The bond coat and the top coat are deposited with a thickness of about 100–150 μm and 250–350 μm , respectively.

2.4. Microstructural Characterization. Cross-sectional samples of dimension $10 \times 5 \times 5 \text{ mm}$ are cut from the coated sample using a low-speed diamond saw (150 low-speed diamond saw, MTI Corporation) for examining the mechanical properties and microstructural characteristics of coatings. The surface characterization of samples is analysed using two microscopes, namely Zeiss Supra 40 field emission scanning electron microscope (FE-SEM) and Zeiss scanning electron microscope (SEM). Before taking SEM, the cross-sectional sample inserts are subjected to thermoplastic cold mount with Geosyn cold mounting compound powder and liquid procured from Geologists Syndicate Private Limited, Kolkata, India. The cold mounted sample inserts are then allowed for surface polishing with three different substances such as SiC abrasive paper (220, 400, 600, 800, and 1,000 grades), diamond paste polishing (grade range 8, 6, 3, and 1 micron), and velvet cloth fixed auto polisher (Struers, LaboPol-21).

2.5. Porosity Measurement. Thermal-sprayed coatings are vulnerable to porosity formation because of the improper fusion between spray substances or gaseous expansion generated on spraying. Therefore, porosity determination is essential in order to observe the effects of variable spray parameters and the appropriateness of coating for its intended purpose. Based on the type of application, low volume or none of the porosity might be endurable. The porosity measurement in this work is carried out as per [29] procedure.

2.6. Wear Characterization. Wear tests have been performed on as-sprayed coatings using Ducom tribometer (wear and friction monitor: TR-20-M24) under different loading conditions (0.5–1.5 kgf) with sliding velocities (0.17–0.5 m/s) for a constant sliding distance of 300 m. Tungsten carbide balls of 6 mm diameter are used as the counter bodies for all tests. The weight loss in the coatings after the wear test is assessed by comparing the weight of samples before and after the wear test with an electronic balance (Mettler Toledo Classic Plus, AB265-s/Fact). The debris formed on the samples during the wear test is manually removed by blowing air while measuring the sample weight after the wear test. The wear test is conducted three times for each load and speed condition to confirm the consistency of results. Furthermore, average weight loss and standard deviation are calculated. It is to be noted that the wear tests are performed in compliance with ASTM G99-05 standards.

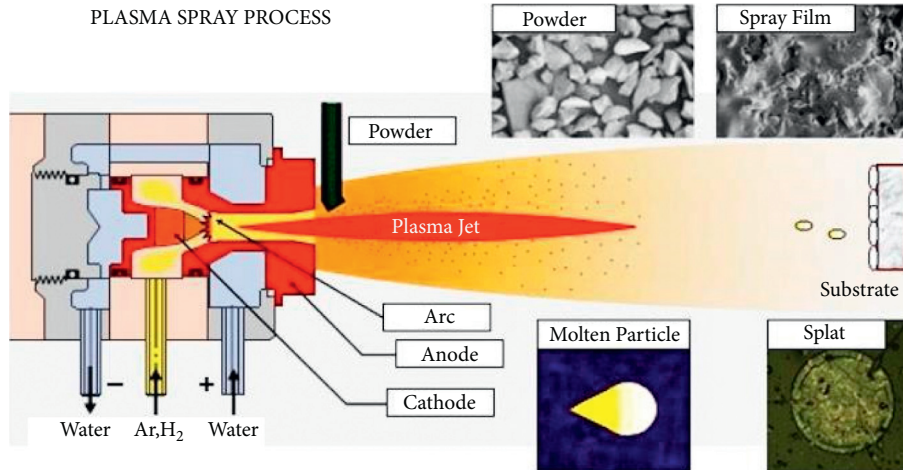


FIGURE 1: Schematic diagram of plasma spraying technique [28].

3. Results and Discussion

3.1. Coating Thickness. The cross-sectional micrographs of CNTs reinforced $\text{Al}_2\text{O}_3 + 3 \text{ wt}\% \text{TiO}_2$ coatings showing coatings thickness are shown in Figure 2. It can be seen from Figure 2 that the coating thickness of the top coat and bond coat are quite different. The average thickness of the top coat is varying in the range of $474\text{--}505 \mu\text{m}$ (Figures 2(a)–2(c)), and the bond coat is obtained with a thickness ranging from 42 to $49 \mu\text{m}$. It can also be observed that the adhesion between the coatings and the substrate is very good, and no cracks were noticed. The EDX analysis of $\text{Al}_2\text{O}_3 + 3 \text{ wt}\% \text{TiO}_2 + 5\% \text{CNTs}$ reinforced coating is shown in Figure 3, and the presence of Ti, C, Al, and so on can be seen in the coating microstructure. Also, the white flakes in the microstructure represent alpha-alumina whereas the sharp edge portions represent titania (Figure 3).

3.2. Phase Analysis. The X-ray diffraction (XRD) patterns for $\text{Al}_2\text{O}_3 + 3 \text{ wt}\% \text{TiO}_2$ composite coatings obtained with and without CNTs reinforcement are shown in Figure 4, and the presence of Al_2O_3 and TiO_2 phases and CNTs can be seen clearly. Through EDX and XRD analysis, the presence of these phases in the coating microstructure has been confirmed. It is to be noted that the alpha-alumina present in the coating resists high-temperature intrusion, and the titania is present in the form of rutile titania. It can be observed that the intensity of peaks in the XRD pattern representing TiO_2 and CNTs is very small as their percentage composition is very less. It can also be seen that the presence of CNTs cannot be seen in the 1% CNTs reinforced coatings due to the smaller volume proportion. It can be observed from the intensity of the phases that the phase distribution is similar in all four types of coatings with slight variation in their quantity.

3.3. Porosity Measurement. Figure 5(a) shows the microstructure of $\text{Al}_2\text{O}_3 + 3 \text{ wt}\% \text{TiO}_2$ coating without adding CNTs, and Figures 5(b)–5(d) show the microstructure of

coatings obtained after the addition of CNTs in 1 wt%, 3 wt%, and 5 wt%, respectively. It is observed from Figures 5(a)–5(d) that micropores are present in the coating microstructure with different sizes. The size of the pores and the number of pores per square millimeter were analysed using MetImage LX software and shown in Figures 5 and 6. It was found that the addition of CNTs reduced the porosity level in the coatings, and this is due to the fact that CNTs are occupying the micropores and resulting in the reduction of the overall porosity percentage.

The variation in porosity in all the coatings is shown in Figure 6. The presence of micropores in size ranges ($0\text{--}10 \mu\text{m}$) occurred more on all coated samples, and gradually, pore volume decreased with an increase in pores size. It can be observed that the 1% CNTs reinforced coating exhibited fewer pores formation than the other coatings, whereas the 3% CNTs reinforced coatings have more pores per square millimeter (see Figure 6). Furthermore, in 5% CNTs reinforced coatings, the number of pores per square millimeter have been decreased. The coating microstructures and MetImage analyzer results indicate that 1% CNTs reinforcement is sufficient for a homogeneous distribution in $\text{Al}_2\text{O}_3 + 3 \text{ wt}\% \text{TiO}_2$ coating, and this can reduce the formation of pores in the coating microstructure effectively. The nonuniform melting and distribution of CNTs in the coating increase the percentage porosity in the coatings. The agglomerates of CNTs in the coating may cause nonuniform CNTs melting and thus resulting in a higher percentage of porosity. It has been observed in previous works also that just the nominal addition of CNTs has supported the alumina to retain the liquid state for a long time and develop the good distribution of alumina in CNTs reinforced alumina-titania composite coatings [30]. It can also be observed that the higher coating thickness has resulted in a higher number of pores formed in the coating microstructure.

3.4. Wear Characteristics. The wear tests are conducted at three different load and speed conditions with a constant sliding distance of 300 m using a steel ball at room temperature. The wear characteristics of the coatings are shown

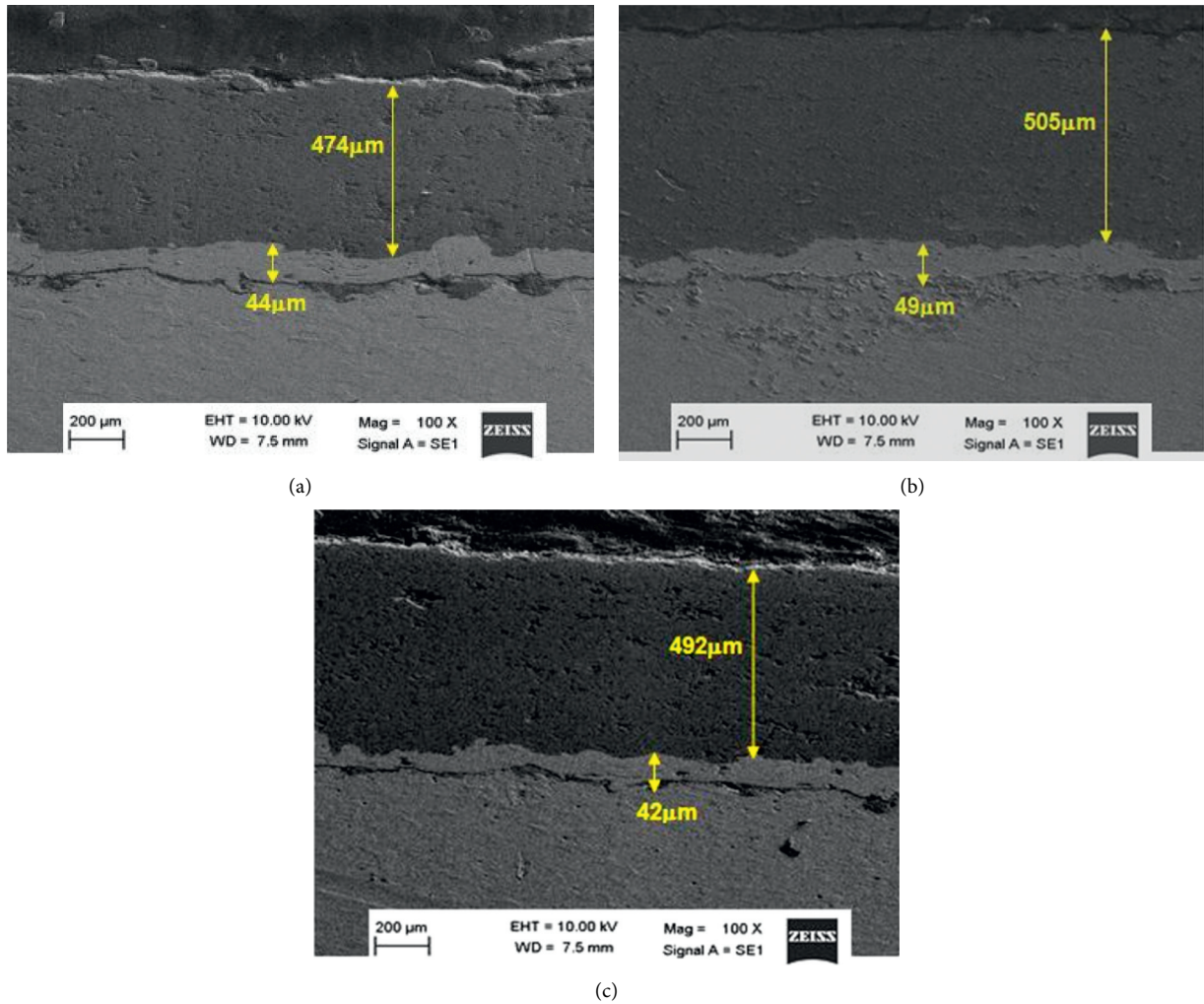


FIGURE 2: SEM micrograph of cross section showing coating thickness of (a) $\text{Al}_2\text{O}_3 + 3 \text{ wt}\% \text{TiO}_2 + 1\% \text{CNTs}$ reinforced coating, (b) $\text{Al}_2\text{O}_3 + 3 \text{ wt}\% \text{TiO}_2 + 3\% \text{CNTs}$ reinforced coating, and (c) $\text{Al}_2\text{O}_3 + 3 \text{ wt}\% \text{TiO}_2 + 5\% \text{CNTs}$ reinforced coating.

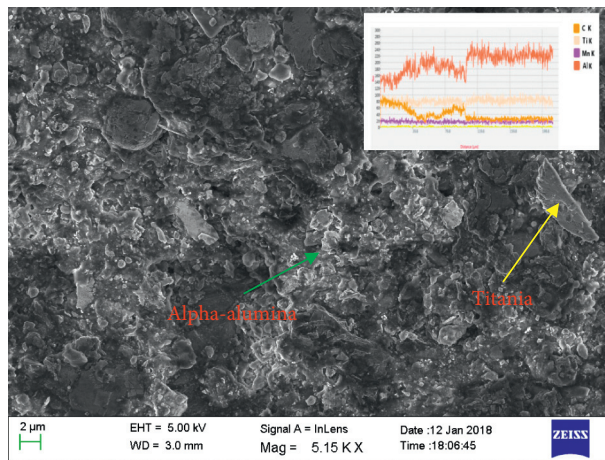
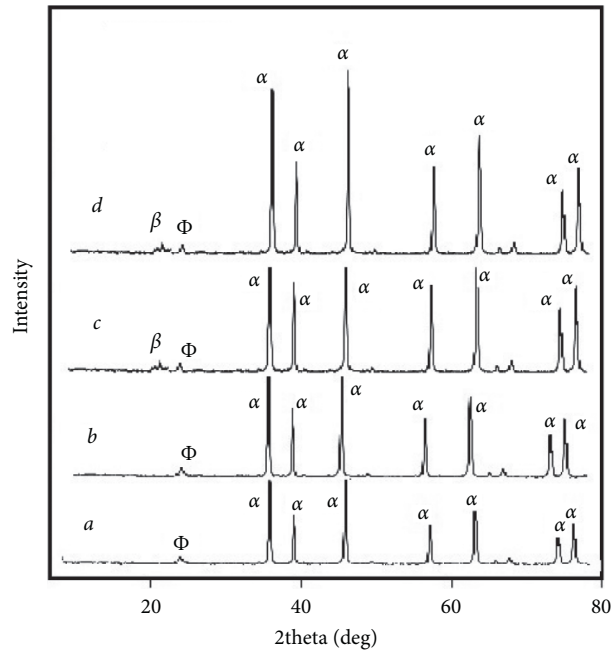


FIGURE 3: SEM micrograph of $\text{Al}_2\text{O}_3 + 3 \text{ wt}\% \text{TiO}_2 + 5\% \text{CNTs}$ reinforced composite coating surface with EDX.

in Figure 7. At 0.17 m/s sliding speed, it can be observed that the weight loss of alumina-titania composite coating without CNTs reinforcement is ranging in between 3.1 and

3.6 mg (Figure 7(a)), whereas for CNTs reinforced coatings, the weight loss is changing from 2.5 to 3.4 mg. It can also be seen that in all the coatings, the weight loss is gradually



β - CNT

α - Al₂O₃

Φ - TiO₂

FIGURE 4: XRD pattern of (a) Al₂O₃ + 3 wt%TiO₂ coating without CNTs reinforcement, (b) Al₂O₃ + 3 wt%TiO₂ + 1% CNTs reinforced coating, (c) Al₂O₃ + 3 wt%TiO₂ + 3% CNTs reinforced coating, and (d) Al₂O₃ + 3 wt%TiO₂ + 5% CNTs reinforced coating.

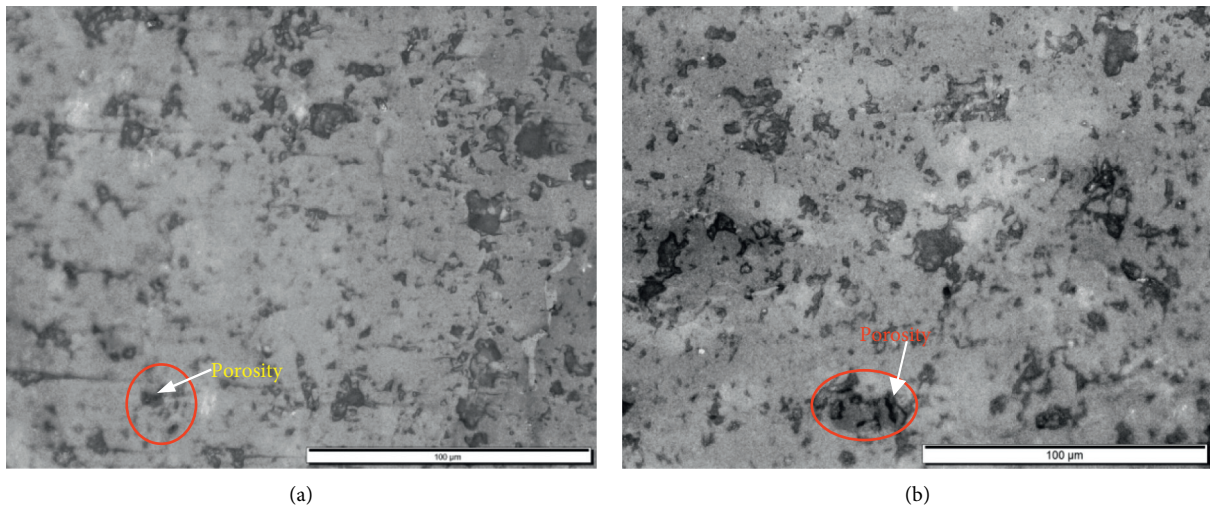


FIGURE 5: Continued.

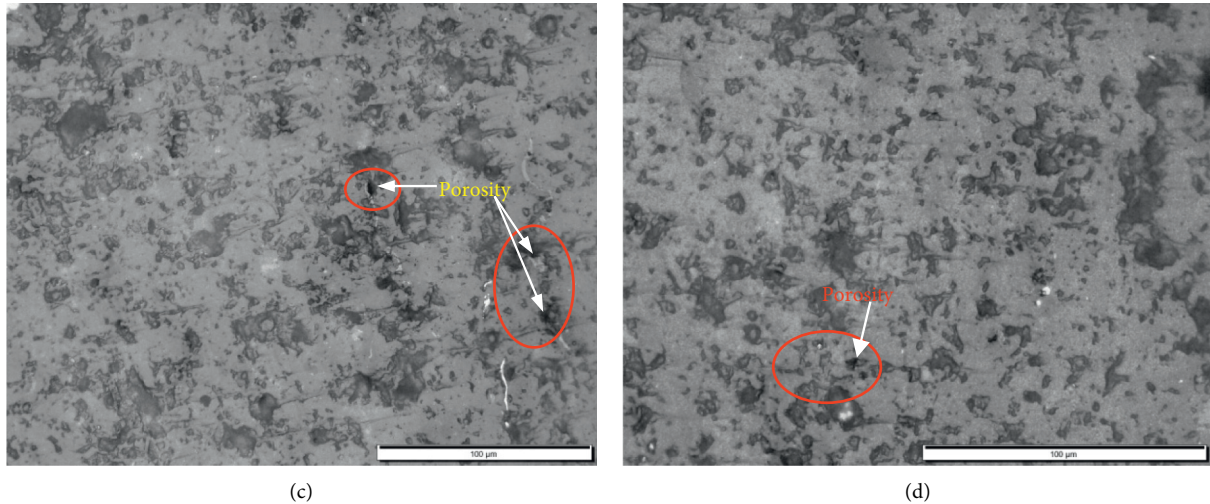


FIGURE 5: Optical micrographs of (a) $\text{Al}_2\text{O}_3 + 3 \text{ wt}\% \text{TiO}_2$ composite coating without CNTs reinforcement, (b) $\text{Al}_2\text{O}_3 + 3 \text{ wt}\% \text{TiO}_2 + 1\%$ CNTs reinforced coating, (c) $\text{Al}_2\text{O}_3 + 3 \text{ wt}\% \text{TiO}_2 + 3\%$ CNTs reinforced coating, and (d) $\text{Al}_2\text{O}_3 + 3 \text{ wt}\% \text{TiO}_2 + 5\%$ CNTs reinforced coating.

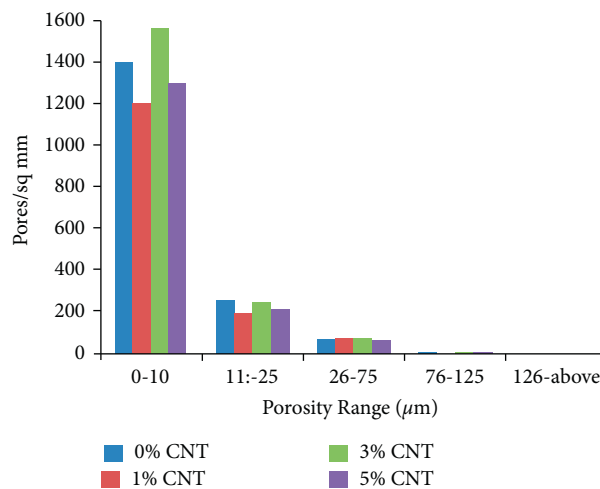


FIGURE 6: Porosity variation in alumina-titania coatings obtained with and without CNTs reinforcement.

increased with the increase of load except a small decrease at 1 kgf load in the case of coatings obtained without CNTs reinforcement.

The wear characteristics obtained at 0.33 m/s sliding speed are shown in Figure 7(b). At this sliding speed also the trend of the variation in weight loss with respect to the load is almost similar. For coatings obtained without CNTs reinforcement, the weight loss is changing from 3.5 to 4.2 mg, whereas for the coatings with CNTs reinforcement, the weight loss is in the range of 2.6–4.3 mg. It can also be observed that there is a short decrease in weight loss at 1 kgf load in the case of 3% CNTs reinforced coatings (Figure 7(b)). Figure 7(c) shows the wear characteristics of coatings at 0.5 m/s sliding speed. At this highest speed, weight loss is in the range of 3.8–4.2 mg for the coatings obtained without CNTs reinforcement, and it shows that wear rate is very much higher at the highest sliding speed. For CNTs reinforced coatings also, the

weight loss is more, and it is in the range of 2.8–3.9 mg. Furthermore, there is a short drop in the weight loss at 1 kg load in the case of 3% CNTs reinforced coatings (Figure 8).

However, it can be clearly seen that the weight loss is increased with the increase in load and sliding velocity. Also, it can be observed that 1 wt% CNTs reinforced coatings exhibited good adhesion of coating with the substrate and resulted in lesser weight loss and thereby higher wear resistance. The factors such as hardness, porosity, and fracture strength might play a significant role in the wear resistance of coatings. It can also be seen that the weight loss in the case of 3 wt% CNTs reinforced coatings and coatings without CNTs reinforcement is almost nearer at all load and speed conditions. Lastly, it can be observed that the weight loss is more in the coatings without CNTs reinforcement, and the weight loss is minimum in the case of 1% CNTs reinforced coatings at all the conditions.

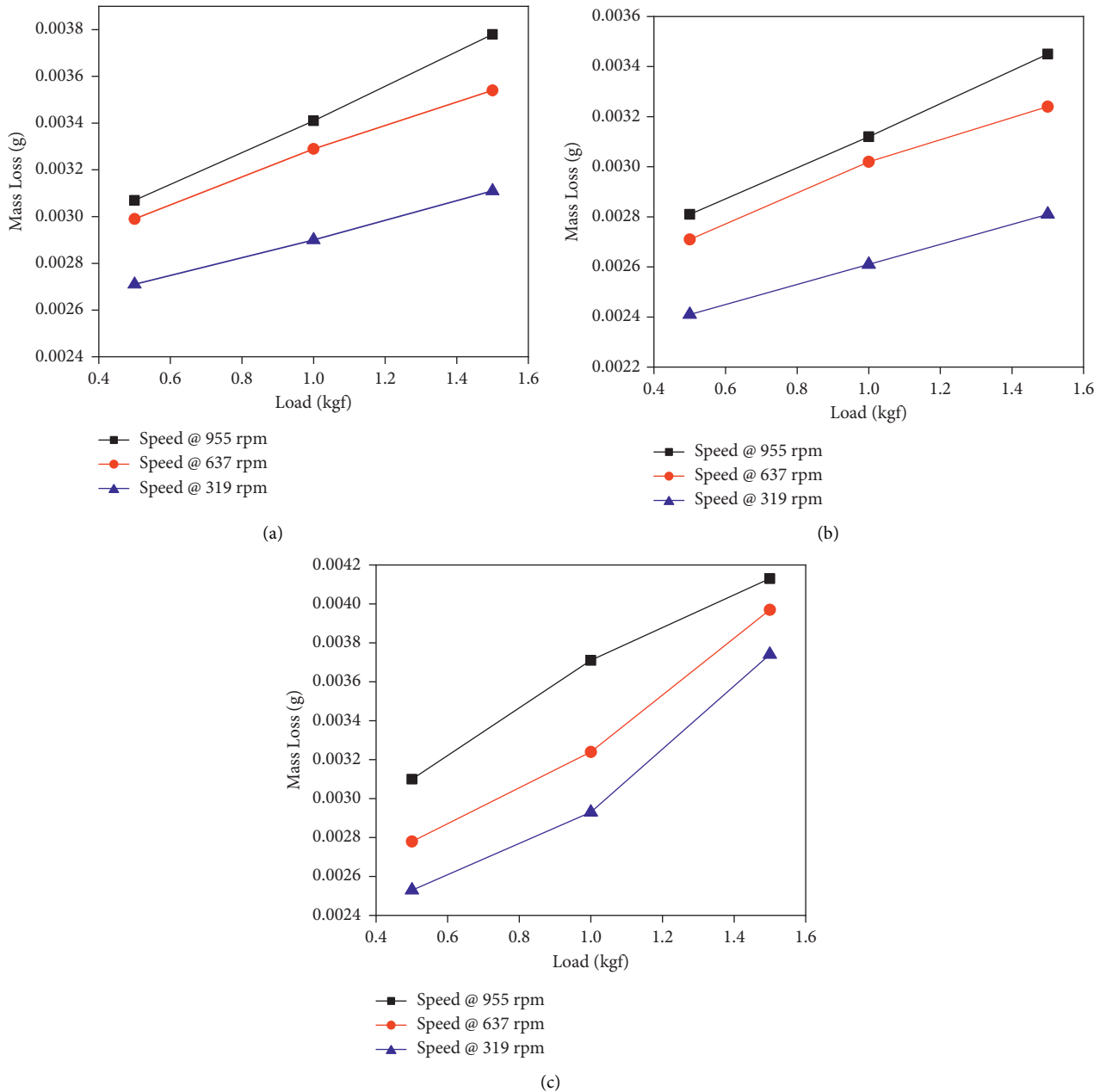


FIGURE 7: Mass loss measured during the experimentation with Al₂O₃ + TiO₂ coating for different rotational speeds: (a) Al₂O₃ + TiO₂ + 1% CNT, (b) Al₂O₃ + TiO₂ + 3% CNT, and (c) Al₂O₃ + TiO₂ + 5% CNT.

The wear resistance is directly proportional to the hardness of the sliding surface. For a rotating ball, the hardness is 85 HRC, and for the Al₂O₃ + TiO₂, it is 65 HRC. Both the materials are rich in hardness compared to the substrate material. During sliding experimentation, in addition to the influence of surface hardness, the frictional energy generated will highly influence to cause wear. In this research, the reinforcement of CNT in the the Al₂O₃ + TiO₂ has simultaneously increased, but in 5%, CNT reinforcement is maintaining the medium value of surface hardness because of more ceramic in the specimen. The behavior of CNT in Al₂O₃ + TiO₂ reveals the performance of diamond during sliding analysis. The maximum wear resistance of 5,800 Nm/

mm³ is recorded for 3% of CNT in Al₂O₃ + TiO₂. Wear resistance is also influenced by the process condition such as applied load and sliding velocity or speed.

3.5. Wear Mechanism. Figure 9 shows the SEM micrographs of wear track obtained on the worn-out surface of Al₂O₃ + 3 wt%TiO₂ coatings reinforced with different percentage proportions of CNTs. Microcracks and fragments of coating are observed on the wear track surface (Figures 9(a) and 9(c)), and more fragments of coating material that came out and fallen on the nearby coating can be seen in Figure 9(b). Also, the deep scratch can be noticed, and no

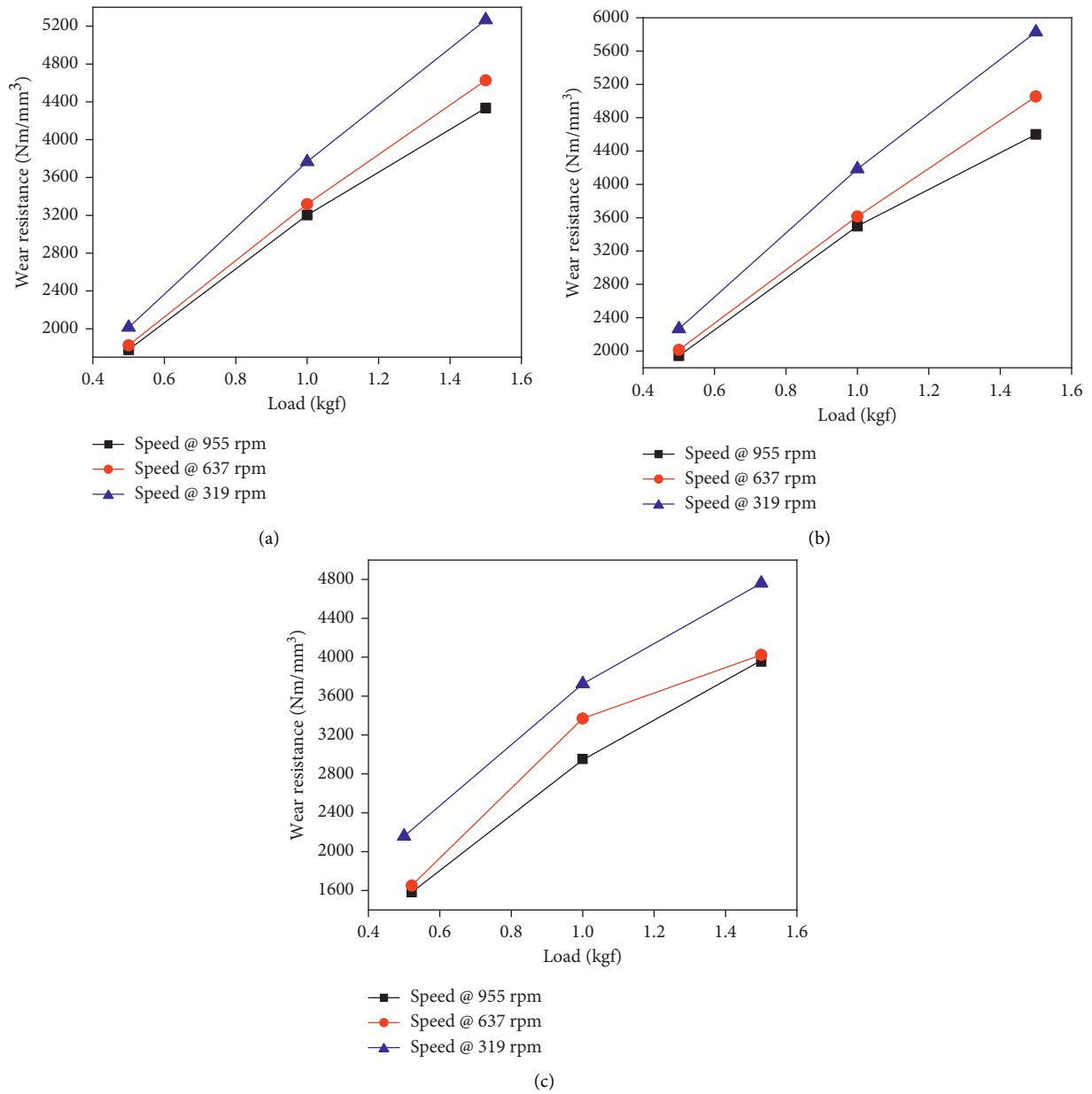


FIGURE 8: Calculated wear resistance for the test experiments on Al₂O₃ + TiO₂ coatings for different rotational speeds: (a) Al₂O₃ + TiO₂ + 1% CNT, (b) Al₂O₃ + TiO₂ + 3% CNT, and (c) Al₂O₃ + TiO₂ + 5% CNT.

cracks are observed (Figure 9(b)). The higher fragmentation of coating and crack formation can be attributed to the poor adhesion strength and low ductility of the coating. However, the higher coating thickness and lower percentage porosity reduced the wear loss of these coatings. However, the 3 wt% CNT addition has reduced the formation of microcracks and also the fragmentation of coating, and this can be attributed to the formation of CNTs bridges in the coating microstructure. Similar types of coating fragments were also noticed on the worn surface by [31].

The SEM micrograph of wear track morphology on the worn-out coating surface is shown in Figure 10. It can be observed that there are many microcracks on the worn surface due to cyclic stresses during the wear tests. The debris

formed in the coating also can be seen (Figure 10(b)). The uniform mixing of CNT particles melted partially in the coating could improve the wear resistance of coatings. The wetting of the CNTs might be one reason for the good dispersion observed. Therefore, the nanotubes that are dispersed in the slurry appear relatively uniformly distributed over the Al₂O₃ + 3 wt%TiO₂ particle surface. The 1 wt% CNTs reinforced Al₂O₃ + 3 wt%TiO₂ coatings are showing the lower porosity minimizing the defects in the worn surface as shown in Figure 10(a). It can also be observed that the wear track width has been increased at a higher load. The wear debris is seen clearly in the 3% reinforced coatings (Figure 10(b)), and the cavities formed in the worn surface are due to the pull-out of coating material. In 5 wt% CNTs

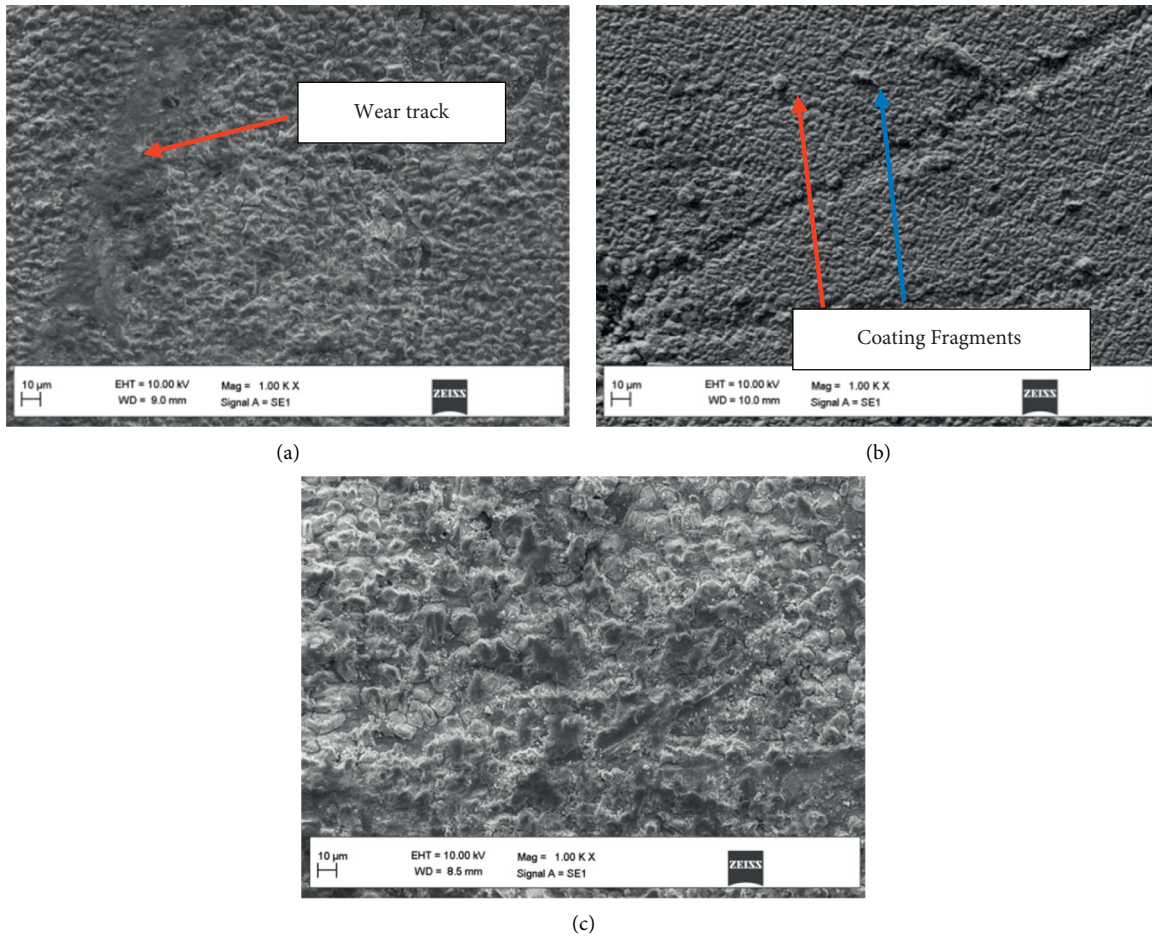


FIGURE 9: SEM micrograph of wear track morphology on the worn-out surface obtained at 0.5 m/s sliding speed and 1 kgf normal load for (a) $\text{Al}_2\text{O}_3 + 3 \text{ wt}\% \text{TiO}_2 + 1 \text{ wt}\% \text{CNTs}$ reinforced coating, (b) $\text{Al}_2\text{O}_3 + 3 \text{ wt}\% \text{TiO}_2 + 3 \text{ wt}\% \text{CNTs}$ reinforced coating, and (c) $\text{Al}_2\text{O}_3 + 3 \text{ wt}\% \text{TiO}_2 + 5 \text{ wt}\% \text{CNTs}$ reinforced coating.

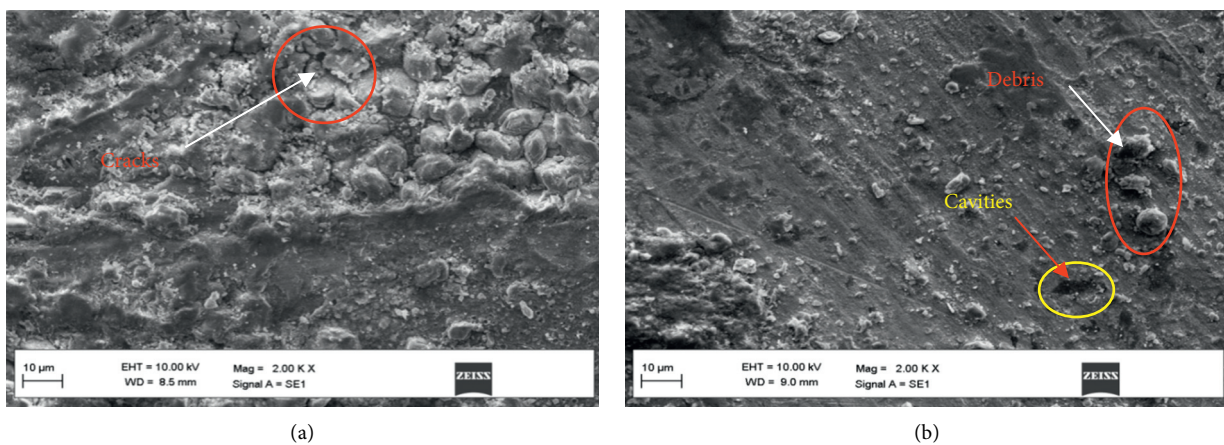
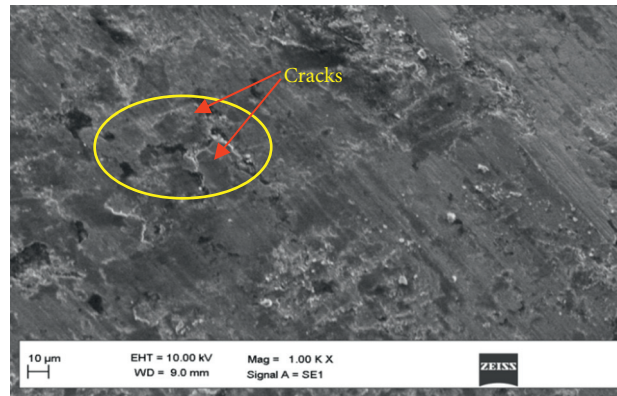


FIGURE 10: Continued.



(c)

FIGURE 10: SEM micrograph of wear track morphology on the worn-out surface obtained at 0.17 m/s sliding speed and 1.5 kgf normal load for (a) $\text{Al}_2\text{O}_3 + 3 \text{ wt}\% \text{TiO}_2 + 1 \text{ wt}\% \text{CNT}$ reinforced coating, (b) $\text{Al}_2\text{O}_3 + 3 \text{ wt}\% \text{TiO}_2 + 3 \text{ wt}\% \text{CNT}$ reinforced coating, and (c) $\text{Al}_2\text{O}_3 + 3 \text{ wt}\% \text{TiO}_2 + 5 \text{ wt}\% \text{CNT}$ reinforced coating.

reinforced coatings, the cracks can be observed on the worn-out surface because of higher load and lesser sliding speed, which resulted in more cyclic stresses in the coating material (Figure 10(c)).

4. Concluding Remarks

In this work, the characteristics of the plasma-sprayed coatings obtained with and without CNTs reinforcement are evaluated and compared. Particularly, the percentage porosity and tribological characteristics of the coatings have been investigated thoroughly. The following conclusions can be drawn from this investigation:

- (1) In all the coatings investigated, the micropores are present in their microstructure, and the percentage porosity is decreased with the increase of the percentage of CNTs. This is due to the metallurgical fusion and surface reaction of CNT with $\text{Al}_2\text{O}_3 + \text{TiO}_2$. As a result, the metallurgical reaction between the elements has simultaneously increased the surface hardness.
- (2) The presence of micropores in 1% and 5% CNTs reinforced $\text{Al}_2\text{O}_3 + 3 \text{ wt}\% \text{TiO}_2$ coatings is minimum, and it has been noticed that the homogeneous distribution of CNTs and formation of CNTs bridges in these coatings have reduced the percentage porosity.
- (3) It is also found that the weight loss in the coatings is more at higher loads and higher sliding speeds due to more cyclic stresses induced in the coating during the wear tests.
- (4) It is observed that the weight loss is gradually reduced with the increase of CNTs reinforcement between 1 and 5 wt%.
- (5) The good adhesion of coating that resulted in lesser weight loss has been observed in the case of 1% CNTs reinforced alumina-titania coatings, whereas in other coatings, very poor adhesion resulting in the formation of cracks has been observed.

- (6) However, it can be clearly seen that the addition of CNTs to the alumina-titania coatings will improve their wear resistance and make them suitable for critical tribological applications.

Data Availability

No data were used to support this study.

Conflicts of Interest

The authors declare that they have no conflicts of interest.

References

- [1] J. Lei, C. Shi, S. Zhou, Z. Gu, and L.-C. Zhang, "Enhanced corrosion and wear resistance properties of carbon fiber reinforced Ni-based composite coating by laser cladding," *Surface and Coatings Technology*, vol. 334, pp. 274–285, 2018.
- [2] F. Wang, F. Zhang, L. Zheng, and H. Zhang, "Structure and corrosion properties of Cr coating deposited on aerospace bearing steel," *Applied Surface Science*, vol. 423, pp. 695–703, 2017b.
- [3] A. Lekatou, D. Sioulas, A. E. Karantzalis, and D. Grimanelis, "A comparative study on the microstructure and surface property evaluation of coatings produced from nanostructured and conventional WC-Co powders HVOF-sprayed on Al7075," *Surface and Coatings Technology*, vol. 276, pp. 539–556, 2015.
- [4] D. Wang, B. Zhang, C. Jia et al., "Influence of carbide grain size and crystal characteristics on the microstructure and mechanical properties of HVOF-sprayed WC-CoCr coatings," *International Journal of Refractory Metals and Hard Materials*, vol. 69, pp. 138–152, 2017a.
- [5] F. Kern, P. Palmero, F. G. Marro, and A. Mestra, "Processing of alumina-zirconia composites by surface modification route with enhanced hardness and wear resistance," *Ceramics International*, vol. 41, no. 1, pp. 889–898, 2015.
- [6] J. Mehta, V. K. Mittal, and P. Gupta, "Role of thermal spray coatings on wear, erosion and corrosion behavior: a review," *Journal of Applied Science and Engineering*, vol. 20, no. 4, pp. 445–452, 2017.

- [7] M. A. Zavareh, A. A. D. M. Sarhan, B. B. A. Razak, and W. J. Basirun, "Plasma thermal spray of ceramic oxide coating on carbon steel with enhanced wear and corrosion resistance for oil and gas applications," *Ceramics International*, vol. 40, no. 9, pp. 14267–14277, 2014.
- [8] M. Peters, C. Leyens, U. Schulz, and W. A. Kaysser, "EB-PVD thermal barrier coatings for aeroengines and gas turbines," *Advanced Engineering Materials*, vol. 3, no. 4, pp. 193–204, 2001.
- [9] G. Mauer, R. Vaßen, and D. Stöver, "Detection of melting temperatures and sources of errors using two-color pyrometry during in-flight measurements of atmospheric plasma-sprayed particles," *International Journal of Thermophysics*, vol. 29, no. 2, pp. 764–786, 2008.
- [10] A. Richter, L. M. Berger, Y. J. Sohn, S. Conze, K. Sempf, and R. Vaßen, "Impact of Al₂O₃-40 wt.% TiO₂ feedstock powder characteristics on the sprayability, microstructure and mechanical properties of plasma sprayed coatings," *Journal of the European Ceramic Society*, vol. 39, no. 16, pp. 5391–5402, 2019.
- [11] P. Carpio, Q. Blochet, B. Pateyron et al., "Correlation of thermal conductivity of suspension plasma sprayed yttria stabilized zirconia coatings with some microstructural effects," *Materials Letters*, vol. 107, pp. 370–373, 2013.
- [12] S. Tailor, M. Singh, R. M. Mohanty, and A. V. Doub, "Microstructural and thermal properties of plasma sprayed YSZ nano-clusters thermal barrier coatings," *Journal of Cluster Science*, vol. 27, no. 5, pp. 1501–1518, 2016.
- [13] N. Curry, N. Markocsan, X. H. Li, A. Tricoire, and M. Dorfman, "Next generation thermal barrier coatings for the gas turbine industry," *Journal of Thermal Spray Technology*, vol. 20, no. 1-2, pp. 108–115, 2011.
- [14] N. Curry, N. Markocsan, L. Östergren, X.-H. Li, and M. Dorfman, "Evaluation of the lifetime and thermal conductivity of dysprosia-stabilized thermal barrier coating systems," *Journal of Thermal Spray Technology*, vol. 22, no. 6, pp. 864–872, 2013.
- [15] F. Cernuschi, "Can TBC porosity be estimated by non-destructive infrared techniques? a theoretical and experimental analysis," *Surface and Coatings Technology*, vol. 272, pp. 387–394, 2015.
- [16] A. Portinha, V. Teixeira, J. Carneiro et al., "Residual stresses and elastic modulus of thermal barrier coatings graded in porosity," *Surface and Coatings Technology*, vol. 188-189, pp. 120–128, 2004.
- [17] A. Kulkarni, A. Golland, H. Herman et al., "Advanced neutron and X-ray techniques for insights into the microstructure of EB-PVD thermal barrier coatings," *Materials Science and Engineering*, vol. 426, no. 1-2, pp. 43–52, 2006.
- [18] W. Chi, S. Sampath, and H. Wang, "Microstructure-thermal conductivity relationships for plasma-sprayed yttria-stabilized zirconia coatings," *Journal of the American Ceramic Society*, vol. 91, no. 8, pp. 2636–2645, 2008.
- [19] Z. Piao, B. Xu, H. Wang, and C. Pu, "Effects of thickness and elastic modulus on stress condition of fatigue-resistant coating under rolling contact," *Journal of Central South University of Technology*, vol. 17, no. 5, pp. 899–905, 2010.
- [20] Z. H. Wen, Y. Bai, J. F. Yang, and J. Huang, "Effect of vacuum re-melting on the solid particles erosion behavior of Ni60-NiCrMoY composite coatings prepared by plasma spraying," *Vacuum*, vol. 134, pp. 73–82, 2016.
- [21] N. Serres, F. Hlawka, S. Costil, C. Langlade, and F. Machi, "Microstructures and environmental assessment of metallic NiCrBSi coatings manufactured via hybrid plasma spray process," *Surface and Coatings Technology*, vol. 205, no. 4, pp. 1039–1046, 2010.
- [22] N. Serres, F. Hlawka, S. Costil, C. Langlade, and F. Machi, "An investigation of the mechanical properties and wear resistance of NiCrBSi coatings carried out by in situ laser remelting," *Wear*, vol. 270, no. 9-10, pp. 640–649, 2011.
- [23] S. Sivaprakasam, M. O. Sikder, L. Ramalingam, G. Kaur, J. M. Dufour, and N. Moustaid-Moussa, "SLC6A14 deficiency is linked to obesity, fatty liver, and metabolic syndrome but only under conditions of a high-fat diet," *Biochimica et Biophysica Acta (BBA)-Molecular Basis of Disease*, vol. 1867, no. 5, Article ID 166087, 2021.
- [24] G. M. T. Basha, A. Srikanth, and B. Venkateshwarlu, "Effect of reinforcement of carbon nanotubes on air plasma sprayed conventional Al₂O₃-3% TiO₂ ceramic coatings," *Materials Today: Proceedings*, vol. 20, pp. 191–194, 2020.
- [25] F. Huang, H. Xu, W. Liu, and S. Zheng, "Microscopic characteristics and properties of titaniferous compound reinforced nickel-based wear-resisting layer via in situ precipitation of plasma spray welding," *Ceramics International*, vol. 44, no. 6, pp. 7088–7097, 2018.
- [26] M. A. Samad and S. K. Sinha, "Mechanical, thermal and tribological characterization of a UHMWPE film reinforced with carbon nanotubes coated on steel," *Tribology International*, vol. 44, no. 12, pp. 1932–1941, 2011.
- [27] K. Nemeth, N. Varro, B. Reti et al., "Synthesis and investigation of SiO₂-MgO coated MWCNTs and their potential application," *Scientific Reports*, vol. 9, no. 1, pp. 15113–15211, 2019.
- [28] Y. Zhang, T. T. Zuo, Z. Tang et al., "Microstructures and properties of high-entropy alloys," *Progress in Materials Science*, vol. 61, pp. 1–93, 2014.
- [29] E2109-01, *Standard Test Methods for Determining Area Percentage Porosity in Thermal Sprayed Coatings*, ASTM International, West Conshohocken, PA, USA, 2014.
- [30] J. G. Thakare, R. S. Mulik, and M. M. Mahapatra, "Effect of carbon nanotubes and aluminum oxide on the properties of a plasma sprayed thermal barrier coating," *Ceramics International*, vol. 44, no. 1, pp. 438–451, 2018.
- [31] K. Yang, J. Li, Q. Wang, Z. Li, Y. Jiang, and Y. Bao, "Effect of laser remelting on microstructure and wear resistance of plasma sprayed Al₂O₃-40% TiO₂ coating," *Wear*, vol. 426, pp. 314–318, 2019.